ChemComm

COMMUNICATION

View Article Online
View Journal | View Issue

Cite this: *Chem. Commun.*, 2023, 59, 9615

Received 11th May 2023,
Accepted 12th July 2023

DOI: 10.1039/d3cc02285d

rsc.li/chemcomm

Three dimensional cyclic trinuclear units based metal–covalent organic frameworks for electrochemical CO_2RR†

Zhenli Liu, [ab] Shichen Yan, *[a] Qianrong Fang, [c] Yaobing Wang [a] and Daqiang Yuan *[a]

A three-dimensional metal–covalent organic framework (3D-MCOF) based on cyclic trinuclear units was synthesized using organic tetrahedral linkers and copper-based cyclic trinuclear complexes. The novel type of 3D-MCOF, named 3D-CTU-MCOF, with the ctn topology, is reported herein for the first time. Our study demonstrated enhanced electrocatalytic capacity for CO_2 reduction reaction of 3D-CTU-MCOF compared to independent cyclic trinuclear units.

In reticular chemistry, extended structures are assembled from building blocks linked by strong bonds.[1] Metal–organic frameworks and covalent-organic frameworks have been widely discussed.[2] It is well known that the dimensions of porous materials influence their porosities and applications.[3] For two-dimensional frameworks, the building units are linked to form layers stacked by weak interactions, resulting in one-dimensional channels.[4] Unlike two-dimensional reticular frameworks, crystalline porous materials with three-dimensional structures generally have interconnecting channels, higher specific surface areas, and porosities.[5] Therefore, applications for crystalline porous materials with three-dimensional structures have attracted great interest.[6]

Functionality is considered critical to leverage their high specific areas and structural tunability.[7] metal–covalent-organic frameworks (MCOFs), which combine coordination chemistry and dynamic covalent chemistry, have generated interest in constructing novel porous materials.[8] In particular, it is important to incorporate functional building blocks into their frameworks; however, constructing functionalized frameworks often requires complex ligand synthesis. Cyclic trinuclear units (CTUs) have received much attention in developing functional coordination complexes due to their potential in various applications.[9] MCOFs can act as proper scaffolds to anchor CTUs, which has been shown to endow MCOFs with innovative functions.[10] However, MCOFs containing CTUs are underreported, particularly those with three-dimensional structures.[11] While planar copper-based CTUs have been efficiently catalytic in 2D MCOFs, few 2D CTU-based frameworks have been reported and have found applications in catalysis.[12] Three-dimensional MCOFs containing CTU have not yet been reported.

Considering these factors, we introduced a 3D-CTU-MCOF based on **ctn** topology. The 3D-CTU-MCOF exhibited high crystallinity and had abundant copper sites in its framework. It exhibited superior performance to the CTUs(Cu_3L) in electrochemical CO_2 reduction reaction (CO_2RR). To our knowledge, this is the first example of three-dimensional CTU-based MCOF.

The construction strategy of 3D-CTU-MCOFs involves two steps that combine coordination chemistry and dynamic covalent chemistry. In Fig. 1a, copper ions are junction points that link 1*H*-pyrazole-4-carbaldehyde through coordination interactions, producing a planar 3-connected building block named Cu_3L. This structure is not commonly seen in MCOFs. Additionally, we utilize 1,3,5,7-tetraaminoadamantane (TAA, Fig. 1b) as the tetrahedral building unit. The combination of Cu_3L and TAA through condensation results in 3D MCOFs, identified as 3D-CTU-MCOF (Fig. 1c). Notably, the 3D-CTU-MCOF adopts a non-interpenetrated **ctn** net, as depicted in Fig. 1d.

3D-CTU-MCOF was synthesized under solvothermal conditions by transferring Cu_3L and TAA into a 5 : 5 (v/v) mixture of 1,4-dioxane and mesitylene with 6 M aqueous acetic acid as a catalyst. Subsequently, the reaction mixture was heated at 120 °C for 3 days, and yellow microcrystalline powders were collected. The structure of 3D-CTU-MCOF was characterized by a range of measurements. The morphology of the as-synthesized

[a] *CAS Key Laboratory of Design and Assembly of Functional Nanostructures, and Fujian Provincial Key Laboratory of Nanomaterials, State Key Laboratory of Structural Chemistry, Fujian Institute of Research on the Structure of Matter, Chinese Academy of Sciences, Fuzhou 350002, Fujian, P. R. China. E-mail: yansch@fjirsm.ac.cn, ydq@fjirsm.ac.cn*
[b] *College of Chemistry and Materials Science, Fujian Normal University, Fuzhou 350007, P. R. China*
[c] *State Key Laboratory of Inorganic Synthesis and Preparative Chemistry, Jilin University, Changchun 130012, China*

† Electronic supplementary information (ESI) available. See DOI: https://doi.org/10.1039/d3cc02285d

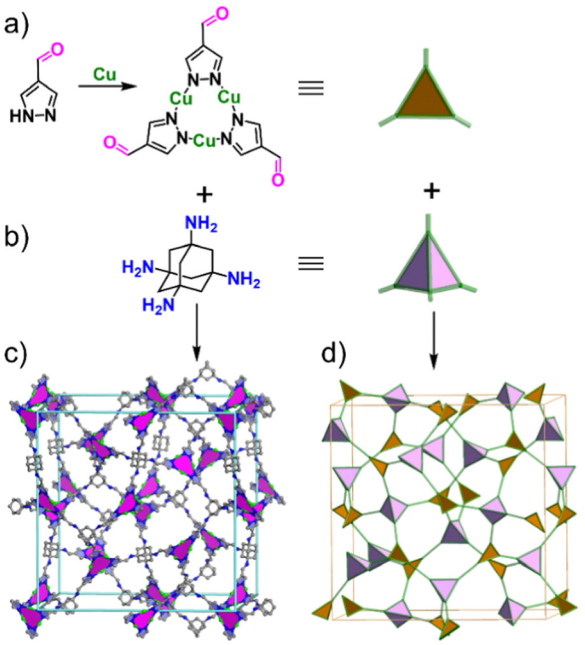

Fig. 1 Illustration of the strategy for building 3D-CTU-MCOF. (a) The mechanism of preparing Cu_3L. (b) The structure of TAA. (c) The crystal structure of 3D-CTU-MCOF (hydrogen atoms are omitted). (d) 3-connected units and 4-connected units to give a **ctn** net of 3D-CTU-MCOF.

3D-CTU-MCOF was studied by scanning electron microscopy (SEM) and transmission electron microscopy (TEM), where rod-shaped crystals of several micrometers were observed (Fig. 2c and d). The integrity of the 3D-CTU-MCOF was investigated by Fourier transform infrared (FT-IR) spectra and solid state ^{13}C cross-polarization magic-angle-spinning (CP/MAS) NMR spectra. The FT-IR spectra (Fig. S1, ESI†) revealed the C═O stretching modes from Cu_3L at 1670 cm^{-1}, and this peak

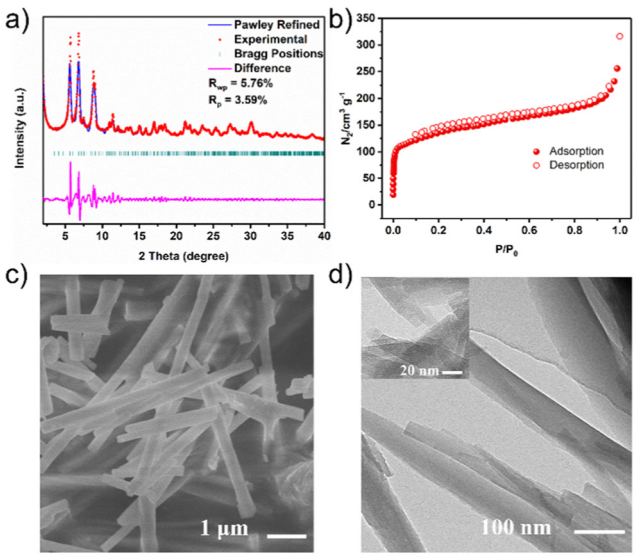

Fig. 2 (a) PXRD patterns of 3D-CTU-MCOF. (b) N_2 adsorption–desorption isotherms of 3D-CTU-MCOF. (c) SEM images of 3D-CTU-MCOF. (d) TEM images of 3D-CTU-MCOF.

became absent after conjugation with TAA. A new peak around 1625 cm^{-1} for 3D-CTU-MCOF indicated the presence of imine bonds.

Additionally, the disappearance of the C═O stretching modes indicated the complete transformation of the formyl groups. In the solid-state NMR spectrum, the chemical shift of 153 ppm, attributed to the presence of C═N, also demonstrated the formation of 3D-CTU-MCOF. The oxidation state of Cu was determined by X-ray photoelectron spectroscopy (XPS), and the binding energy of 932.8 eV implied the presence of Cu(I) ions in this framework, and the Cu 2p binding energy of 934.8 eV could be assigned to Cu(II) due to partial surface oxidation (Fig. S7, ESI†). Additionally, the TGA curve demonstrated that the 3D-CTU-MCOF decomposed at around 177 °C (Fig. S3, ESI†). When the sample was immersed in various organic solvents and water for 24 h, PXRD analyses demonstrated that its crystallinity was still preserved (Fig. S5, ESI†).

The crystal structure of 3D-CTU-MCOF was determined by powder X-ray diffraction analysis, and its structural model adopting the **ctn** topology was simulated using Materials Studio software. As a result, it crystallized in the cubic space group, $I\bar{4}3_d$ ($a = b = c = 37.8218$ Å and $\alpha = \beta = \gamma = 90°$). Moreover, full profile pattern matching (Pawley) refinements were also carried out on the experimental PXRD patterns. The refinement results matched well with the observed patterns ($R_{\omega p}$ = 5.76% and R_p = 3.59%) (Fig. 2a). Peaks at 5.69, 6.82, 7.50, 8.81 and 11.44° correspond to the (211), (220), (310), (321) and (332) Bragg peaks. We investigated the alternative structure based on the **bor** net. As shown in Fig. S4 (ESI†), the experimental pattern did not agree with the simulated one. These results further corroborated that the 3D-CTU-MCOF adopted the expected **ctn** topology. The specific surface area and porosity were characterized by N_2 adsorption and desorption measurements (Fig. 2b). The type I isotherm indicated its microporous character, consistent with the pore size distribution (Fig. S6, ESI†). The Brunauer–Emmett–Teller (BET) surface area and pore size were 424 $m^2\ g^{-1}$ and 1.4 nm, respectively, which agreed with the proposed structural model. Notably, the 3D-CTU-MCOF showed a non-interpenetrated **ctn** topology which will facilitate the development of three-dimensional metal covalent organic frameworks.

Encouraged by the interesting results mentioned above, we further explored its performance in electrochemical CO_2RR. It is well known that CO_2, an abundant source of C1, can be catalytically converted to carbon-based chemicals using copper-containing catalysts. Herein, we propose that 3D-CTU-MCOF with active Cu sites may be suitable for electrochemical CO_2RR. Compared to independent Cu-based CTU, the 3D-CTU-MCOF may have a better activity that can be tuned through the framework formation.

In general, the electrochemical CO_2RR measurements of 3D-CTU-MCOF were performed using a standard three-electrode setup with a carbon paper working electrode, a platinum sheet counter electrode, and Ag/AgCl as the reference electrode. As shown in Fig. 3a, 3D-CTU-MCOF exhibited an enhanced current density in a CO_2-saturated electrolyte

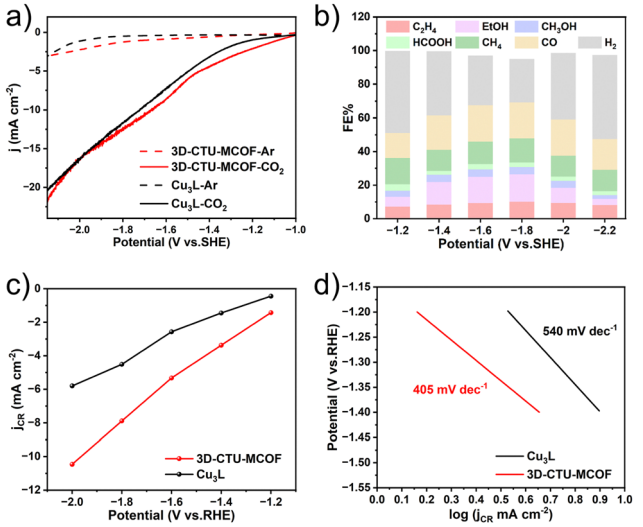

Fig. 3 ECO_2RR activity evaluation of 3D-CTU-MCOF. (a) LSV curves of two catalysts in CO_2/Ar-saturated 0.1 M $EmimBF_4$-MeCN solutions. (b) ECO_2RR FEs for 3D-CTU-MCOF at different potentials. (c) j_{CR} for two catalysts. (d) Tafel plots for j_{CR}.

compared to that in an argon-saturated electrolyte. Moreover, 3D-CTU-MCOF showed a more significant current density than Cu_3L over a potential range of −1 to −2.15 V *vs.* SHE in an argon-saturated electrolyte. Besides, in a CO_2-saturated electrolyte (0.1 M $EmimBF_4$-MeCN solution), the initial potential of 3D-CTU-MCOF showed a positive shift. All results indicated lower reduction overpotential and better performance of 3D-CTU-MCOF compared to Cu_3L.

The product analysis was carried out using gas chromatography and ion chromatography. The total faradaic efficiency (FE) of carbon-based products with 3D-CTU-MCOF as the catalyst remained above 50% throughout the applied potential range (−1.2 V ∼ −2.2 V *vs.* SHE) (Fig. 3b), which was significantly higher than that with Cu_3L as the catalyst (Fig. S9, ESI†). The FE of the carbon products reached 69.2% at −1.8 V *vs.* SHE, with an FE of 26.4% for C_2 products. As shown in Fig. 3c, the partial current densities for both materials were dependent on the applied potential, and the higher density for 3D-CTU-MCOF indicated a higher CO_2 reduction efficiency. The Tafel slope of 405 mV dec^{-1} for 3D-CTU-MCOF was smaller than that for Cu_3L (540 mV dec^{-1}), implying that 3D-CTU-MCOF was more favourable for CO_2 reduction in the kinetic process than Cu_3L (Fig. 3d). The electrochemically accessible surface area (ECSA) of 1.22 mF cm^{-2} for 3D-CTU-MCOF was higher than that of 1.13 mF cm^{-2} for Cu_3L, demonstrating the higher catalytic activity of 3D-CTU-MCOF (Fig. S8, ESI†). The ICP analysis revealed no copper ions in the filtrate after the electrolysis. In addition, the EIS results also indicated that 3D-CTU-MCOF had a superior kinetic property (Fig. S10, ESI†).

In conclusion, we have introduced the copper-based cyclic trinuclear units into three-dimensional metal covalent organic frameworks for the first time. A new CTU-based MCOF adopting **ctn** topology was successfully prepared and showed high crystallinity. Furthermore, 3D-CTU-MCOF displayed better catalytic activity than Cu_3L in electrochemical CO_2RR. The results suggest combining coordination and dynamic covalent chemistry to anchor active sites in the backbone can improve catalytic activity. Moreover, the successful preparation of 3D-CTU-MCOF paves the way for constructing three-dimensional functionalized crystalline porous materials.

This work was supported by the National Natural Science Foundation of China (No. 21872147, 22022110, 22279141, and 22101149), the Key Research Program of Frontier Sciences, CAS (No. ZDBS-LY-SLH028), National Key Research & Development Program of China (2021YFA1501501), Fujian Science & Technology Innovation Laboratory for Optoelectronic Information of China (No. 2021ZZ106).

Conflicts of interest

There are no conflicts to declare.

Notes and references

1 (*a*) O. M. Yaghi, *J. Am. Chem. Soc.*, 2016, **138**, 15507–15509; (*b*) H. Lyu, Z. Ji, S. Wuttke and O. M. Yaghi, *Chemistry*, 2020, **6**, 2219–2241.
2 (*a*) C. A. Trickett, A. Helal, B. A. Al-Maythalony, Z. H. Yamani, K. E. Cordova and O. M. Yaghi, *Nat. Rev. Mater.*, 2017, **2**, 17045; (*b*) K. Geng, T. He, R. Liu, S. Dalapati, K. T. Tan, Z. Li, S. Tao, Y. Gong, Q. Jiang and D. Jiang, *Chem. Rev.*, 2020, **120**, 8814–8933.
3 (*a*) Y. Meng, Y. Luo, J. L. Shi, H. Ding, X. Lang, W. Chen, A. Zheng, J. Sun and C. Wang, *Angew. Chem., Int. Ed.*, 2020, **59**, 3624–3629; (*b*) X. Feng, Y. Song and W. Lin, *J. Am. Chem. Soc.*, 2021, **143**, 8184–8192.
4 (*a*) A. K. Mohammed, P. Pena-Sánchez, A. Pandikassala, S. Gaber, A. A. AlKhoori, T. Skorjanc, K. Polychronopoulou, S. Kurungot, F. Gándara and D. Shetty, *Chem. Commun.*, 2023, **59**, 2608–2611; (*b*) L. Majidi, A. Ahmadiparidari, N. Shan, S. N. Misal, K. Kumar, Z. Huang, S. Rastegar, Z. Hemmat, X. Zou, P. Zapol, J. Cabana, L. A. Curtiss and A. Salehi-Khojin, *Adv. Mater.*, 2021, **33**, e2004393.
5 (*a*) X. Guan, F. Chen, Q. Fang and S. Qiu, *Chem. Soc. Rev.*, 2020, **49**, 1357–1384; (*b*) R. Wang, B. C. Bukowski, J. Duan, J. Sui, R. Q. Snurr and J. T. Hupp, *Chem. Mater.*, 2021, **33**, 6832–6840.
6 (*a*) Z. Lu, J. Liu, X. Zhang, Y. Liao, R. Wang, K. Zhang, J. Lyu, O. K. Farha and J. T. Hupp, *J. Am. Chem. Soc.*, 2020, **142**, 21110–21121; (*b*) X. Wang, Z. Niu, A. M. Al-Enizi, A. Nafady, Y. Wu, B. Aguila, G. Verma, L. Wojtas, Y.-S. Chen, Z. Li and S. Ma, *J. Mater. Chem. A*, 2019, **7**, 13585–13590; (*c*) X. L. Lv, L. Feng, K. Y. Wang, L. H. Xie, T. He, W. Wu, J. R. Li and H. C. Zhou, *Angew. Chem., Int. Ed.*, 2021, **60**, 2053–2057.
7 (*a*) Q. Guan, L. L. Zhou and Y. B. Dong, *Chem. Soc. Rev.*, 2022, **51**, 6307–6416; (*b*) L. Chen, R. Luque and Y. Li, *Chem. Soc. Rev.*, 2017, **46**, 4614–4630.
8 (*a*) J. Dong, X. Han, Y. Liu, H. Li and Y. Cui, *Angew. Chem., Int. Ed.*, 2020, **59**, 13722–13733; (*b*) W. K. Han, Y. Liu, X. D. Yan and Z. G. Gu, *Mater. Chem. Front.*, 2023, DOI: **10.1039/d3qm00020f**; (*c*) M. C. Ma, X. F. Lu, Y. Guo, L. C. Wang and X. J. Liang, *TrAC, Trends Anal. Chem.*, 2022, **157**, 116741.
9 J. Zheng, Z. Lu, K. Wu, G. H. Ning and D. Li, *Chem. Rev.*, 2020, **120**, 9675–9742.
10 X. Li, J. Wang, F. Xue, Y. Wu, H. Xu, T. Yi and Q. Li, *Angew. Chem., Int. Ed.*, 2021, **60**, 2534–2540.
11 (*a*) J. Zhou, J. Li, L. Kan, L. Zhang, Q. Huang, Y. Yan, Y. Chen, J. Liu, S. L. Li and Y. Q. Lan, *Nat. Commun.*, 2022, **13**, 4681; (*b*) R. J. Wei, P. Y. You, H. Duan, M. Xie, R. Q. Xia, X. Chen, X. Zhao, G. H. Ning, A. I. Cooper and D. Li, *J. Am. Chem. Soc.*, 2022, **144**, 17487–17495; (*c*) J. Luo, X. Luo, M. Xie, H. Z. Li, H. Duan, H. G. Zhou, R. J. Wei, G. H. Ning and D. Li, *Nat. Commun.*, 2022, **13**, 7771.
12 (*a*) R.-J. Wei, H.-G. Zhou, Z.-Y. Zhang, G.-H. Ning and D. Li, *CCS Chem.*, 2021, **3**, 2045–2053; (*b*) H. G. Zhou, R. Q. Xia, J. Zheng, D. Yuan, G. H. Ning and D. Li, *Chem. Sci.*, 2021, **12**, 6280–6286.